A simulation method of thermo-hydraulic coupling transfer in soil freeze-thaw process based on the water physical phase change

Ceting Yu[1,2], Fugang Wang[1,2*], Lujiao Ding[1,2], Guanhong Feng[1,2*],Hui Cheng[1,2], Yaohui Wang[1,2], Zhongle Cheng[1,2], Jingwei Sun[1,2]

1. Key Laboratory of Groundwater Resources and Environment, Ministry of Education, Jilin University, Changchun 130012, China
2. Jilin Province Key Laboratory of Water Resources and Water Environment, Changchun 130012, China

Corresponding author: Fugang Wang (wangfugang@jlu.edu.cn). Guanhong Feng(guanhong_feng@jlu.edu.com).

Key Points：

- A new coupling method was proposed to simulate the freeze-thaw process.
- The reliability of the method was verified by the field monitoring data.
- The permeability model and the thermal conductivity model were improved.

Abstract

The freeze-thaw process influences moisture and heat transport, which is of great importance to the runoff and groundwater infiltration processes. At present, the research on the freeze-thaw process is mainly conducted by means of field/laboratory experiments. The mechanism and details of the fluid and heat flow characteristics are still poorly understood. In this study, we developed the code to realize the elaborate description of each thermo-hydraulic phenomenon during the entire freeze-thaw process. Based on the framework of TOUGH2, we improved the EOS3 module to realize the function of phase transition between water and ice. The improved model can handle the system of water/air two components in gas/liquid/solid three phases. Moreover, the absolute and relative permeability change and thermal conductivity correction induced by the occurrence of the ice phase are all considered. The long-term field monitoring was conducted on two sites to observe the entire freeze-thaw process in the Changbai Mountain area. The monitoring data were used to verify the code and get a satisfactory result. It is found that the freeze-thaw process could be briefly divided into three stages, the gradually freezing stage, long-term stable stage, and a prompt thaw stage. The proposed method provides a solution for the in-depth investigation of the moisture and heat migration, and groundwater dynamics in seasonally frozen areas.

1. Introduction

Seasonally frozen soil is widely distributed around the world, where surface ecology, soil structure and hydrological processes in the seasonally frozen soil area are significantly different under freeze-thaw conditions(Hou et al., 2020; Knighton et al., 2019; Kong et al., 2022; Liu et al., 2022; B. Sun et al., 2022; Walvoord & Kurylyk, 2016; Walvoord et al., 2012; X. Wang et al., 2020). The freeze-thaw process have a strong impact on the distribution of heat and moisture in cold regions(Hansson et al., 2004; Nikolaev et al., 2022; Painter et al., 2016; Peng et al., 2016; Stuurop et al., 2021). However, there are challenges in modeling the complex thermo-hydrologic process in the simulation, especially in the data-scared area (Ireson et al., 2013; Kurylyk & Watanabe, 2013; Painter et al., 2013). Therefore, an accurate simulation method of thermo-hydraulic coupling transfer under the freeze-thaw process is needed.

The frozen soil system consists of air, pore water, pore ice and soil skeleton. Affected by the alternate change in air temperature and precipitation in cold regions, water freezing or ice crystal melting caused by continuous migration and accumulation of water can significantly cause the spatial redistribution of ice-water-soil skeleton system(Nagare et al., 2012; D. Y. Wang et al., 2018) and change the physical and mechanical properties of the foundation soil(Chen et al., 2021; Christ & Kim, 2009; Ebel et al., 2019; Orakoglu et al., 2016). Temperature and water content are the most important factors in determining the presence of unfrozen water and ice. Below 0℃, temperature gradient is the driving force of moisture migration. Simultaneously, the variation of ice-water-soil skeleton proportion will lead to a dramatically change on thermal conductivity and specific heat capacity(He,

Flerchinger, Kojima, He, et al., 2021; Sjoberg et al., 2016), which will influence heat transport inversely. Generally, it is assumed that ice has a thermal conductivity between 2.1 and 2.4 J $m^{-1}s^{-1}℃^{-1}$ and a specific heat capacity between 1, 800 and 2, 100 J $kg^{-1}℃^{-1}$, while liquid water has a thermal conductivity of between 0.54 and 0.60 J $m^{-1}s^{-1}℃^{-1}$ and a specific heat capacity between 4, 180 and 4, 190 J $kg^{-1}℃^{-1}$. In recent years, much attention have been paid on the research of moisture and heat migration during the freeze-thaw process, which will substantially affect hydrological processes such as surface runoff processes and groundwater infiltration processes(Bense et al., 2009; Devoie et al., 2020; Kurylyk et al., 2016; Rush & Rajaram, 2022; Sutton & Price, 2020; Walvoord & Kurylyk, 2016; Walvoord et al., 2012). Therefore, studying of the coupled moisture and heat transport processes in seasonally frozen area is becoming increasingly necessary.

Based on the principle of liquid water viscous flow and heat balance in porous media, Philip and Vries (1957)first proposed a coupled hydrothermal migration model suitable for unsaturated zones. According to the law of Richards(1931) equation and energy conservation principle, Harlan (1973)first proposed the model of heat, mass and moisture migration in the process of soil freezing and gave a numerical solution to the problem using finite differences. A series of mathematical models suitable for the thermo-hydraulic process was developed in past years(Hansson et al., 2004; Kurylyk et al., 2014; Painter et al., 2016; Zhang et al., 2021). There are also models that couple solute transport(Frederick & Buffett, 2016; Mohammed et al., 2021; L. Wang et al., 2021; Yi et al., 2021) and mechanical deformation, which the coupled hydrothermal equations are predicated on the conservation principles of fluid mass and energy as same as the coupled hydrothermal models.

A lot of professional softwares were developed to simulate the hydrogeological multiphase flow system. To compare and validate the different simulators of groundwater flow and heat transport in cold regions, an international collaborative benchmarking initiative (InterFrost) was launched in 2014(Grenier et al., 2018). Thirteen codes including ATS(Painter et al., 2016), DarcyTools(Langford et al., 2020), FELOW, SMOKER(Dagenais et al., 2020), PFLOTRAN(Karra et al., 2014), MELT(Frederick & Buffett, 2014), GEOAN(Holmen et al., 2011), Ginette(Riviere et al., 2019), SUTRA(McKenzie et al., 2007), implement in COMSOL(Scheidegger et al., 2019), PermaFOAM(Orgogozo et al., 2019), Cast3M(Grenier et al., 2013), PlexPDE(Bense et al., 2009) were tested and compared in multiple benchmarking scenarios. Besides aboved codes, GeoTop(Endrizzi et al., 2014), MarsFlo(Painter, 2011), HYDRUS-1D(Zhao et al., 2016), SHAW(Flerchinger & Hanson, 1989) models are also used widely in the simulation of hydrogeological flow system in cold regions. For most models, the govering equations are similar, the unknown varibles which effect the hydrothermal coupling model as well as temperature-dependent thermal properties and hydraulic conductivities include the content of unfrozen water, pore ice content and temperature. Non-linear effects will be induced due to the variation in coefficient with the moisture migration and heat migration. Therefore, it is necessary to introduce a reasonable method to recouple the hydrothermal coupling model. The models aboved vary greatly in their coupling approach, or, in other words, how the

moisture content influences the temperature mutually.

The copuling approach can be divided into the empirical approaches and mechanistic approaches roughly(Lamontagne-Halle et al., 2020). The empirical approach relies on a function defining a relationship between the temperature and the liquid water content in subzero conditions. While the chosen functions are usually obtaind by laboratory experiments and can be a linear function(McKenzie et al., 2007), a power function(Kurylyk & Hayashi, 2016) or an exponential function(Evans et al., 2018).The mechanistic approach uses a generalized Clausius–Clapeyron equation to combine the soil freezing characteristic curve(SFCC) (Dall'Amico et al., 2011; Hansson et al., 2004). However, to prevent the soil from completely freezing, a minimum water content limit is usually set artificially in the SFCC function(Ghias et al., 2019; McKenzie et al., 2007). Wether the empicrical approach or the artificial estimation in the parameteration of SFCC functions is lack of physically reasonable description, in other words , the unfrozen water content doesn't depend on the thermodynamic properties of the fluid phases of water substance over a wide range of conditions.

TOUGH2 is a specialized program widely used in the simulation of hydrothermal process for multiphase fluids in many fields(Seyedrahimi-Niaraq et al., 2021; D.-m. Sun et al., 2016; Y. Sun et al., 2019), which can't be used in the same process under freeze-thaw conditions due to the reason that the EOS3 module in TOUGH2 can only describe the gas/water two-phase flow in unsaturated zone which doesn't consist of ice phase. In this study, we coupled the improved EOS module into the TOUGH2 for considering the hydrothermal migration and the water phase change behavior during freeze-thaw process.

In the improved EOS module, IAPWS-IF97 is employed for the calculation of water properties. IAPWS-IF97 is the formulation for the thermodynamic properties of water and steam for industrial use adopted by the International Association for the Properties of Water and Steam (IAPWS) in 1997. A non-isothermal hypothesis and a new model of permeability is introduced into the simulator, which helps accurately describe the multiphase flow behavior under freeze-thaw process more reliably. This study provides a solution for the distributation of moisture content and temperature of the soil, and the frozen depth during freeze-thaw process.

2. Material and method

2.1 Study area and site monitoring

The study area is located in Fusong County, Baishan City, southeastern Jilin Province (127°01'-128°06'E, 41°42'-42°49'N, covering an area of 6159 square kilometers). This area has a characteristic of a cold-temperate zone continental monsoon, with four distinct seasons and an uneven precipitation distribution(H. Wang et al., 2023). The temperature difference within a year could reach up to 70ºC. According to the data of meteorological stations in Baishan City, the average annual temperature is 3.8 -- 7℃, and the lowest temperature is in January, whose monthly average temperature is about -20℃, with a minimum of -40ºC. The highest

temperature is in July, whose monthly average temperature is around 23℃, and the maximum could reach 37℃. The annual precipitation ranges from 750 to 1300mm, most of which occurs from June to September, accounting for 70-80% of the year. The average surface evaporation is 1000-1200mm/year. The region has a frost-free period of 60-132 days and the maximum freezing depth of the region is 1.62-2.34m. The annual average sunshine hours are 2400 hours. The temperature and precipitation data of the area within the study period are shown in Figure 1.

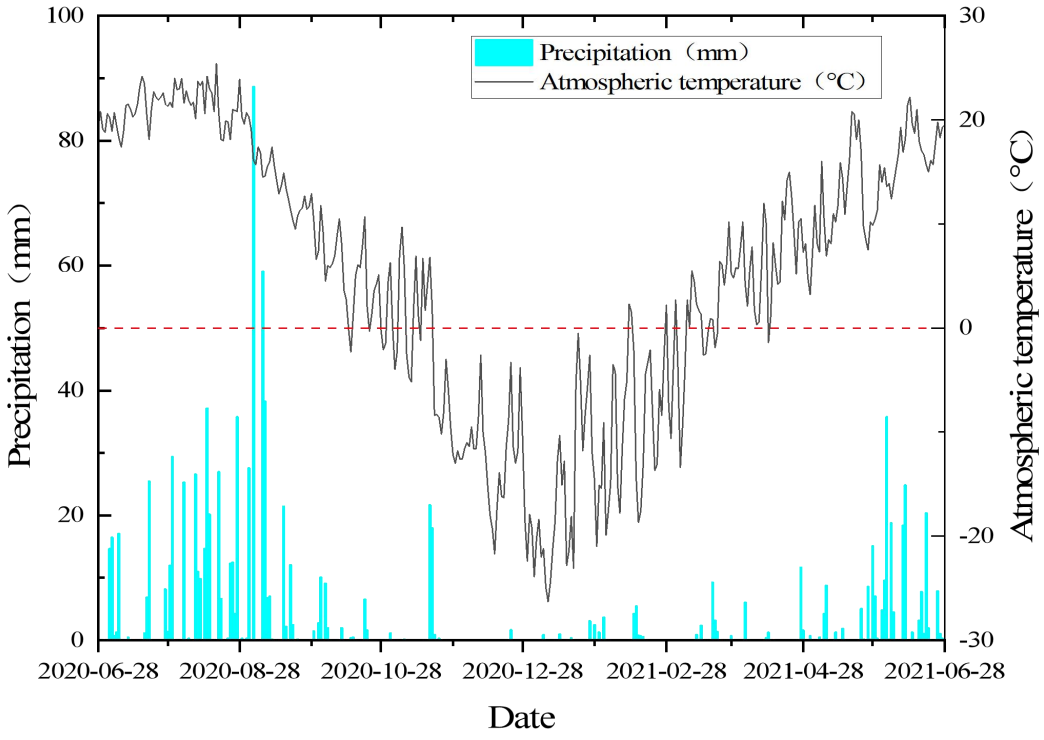

Figure 1. Meteorological data of the study area

Two soil monitoring sites, T01 (127°4'43.3056"E, 42°23'47.1156"N) and T02 (127°30'41.5764"E, 42°10'39.6588"N), are set up to record the variation in temperature and moisture content as shown in Figure 2. The stratigraphic profile diagram of the monitoring sites is shown in Figure 3. The surface humus soil is 40cm thick and contains plant roots. In descending order, The thickness of yellow-brown sandy silt is 20cm and the thickness of earthy yellow silty clay silt is 60cm with high humidity. The layout of the two monitoring sites is the same, with the monitoring points located 20cm, 40cm, 70cm, 100cm, and 150cm beneath the ground. TDR probe was used to measure the temperature and moisture content of each node in real-time. The TDR probe model is TEROS 12 soil moisture, temperature and conductivity sensor, measuring frequency is 70MHz, length of the probe is 5.5cm.

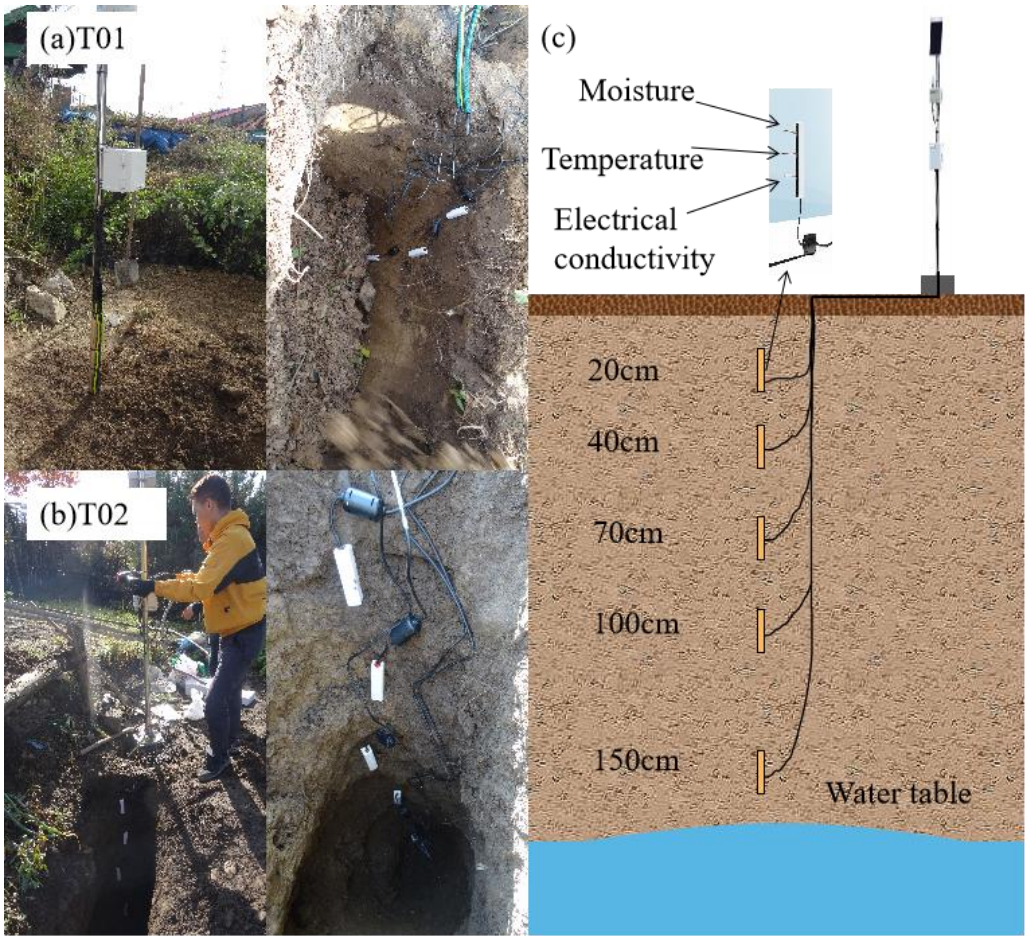

Figure 2. Photos of the in-situ soil monitoring device and sensor placement at (a) T01 and (b) T02; ;(c): Schematic diagram of soil monitoring profile.

2.2 Monitoring data and division of freeze-thaw cycles

The time range of the measurements is from October 12, 2020 to June 8, 2021, and the TDR probe acquired a set of moisture content and temperature data each half hour. The meteorological data (rainfall and surface temperature data) of the study area are from the measured data of Jingyu Donggang Station in Baishan City. The changes in temperature and moisture content at different layers of the two monitoring sites are shown in Figure 3 and Figure 4.

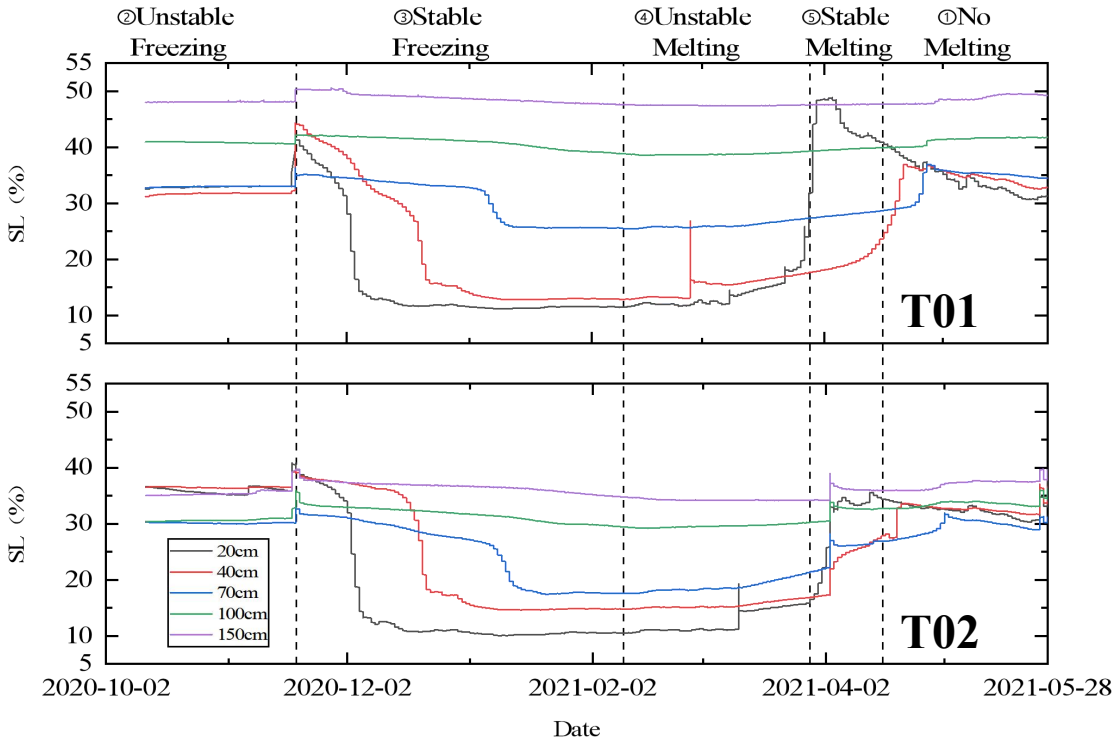

Figure 3. The soil moisture content monitoring curves of T01 and T02 at different depths

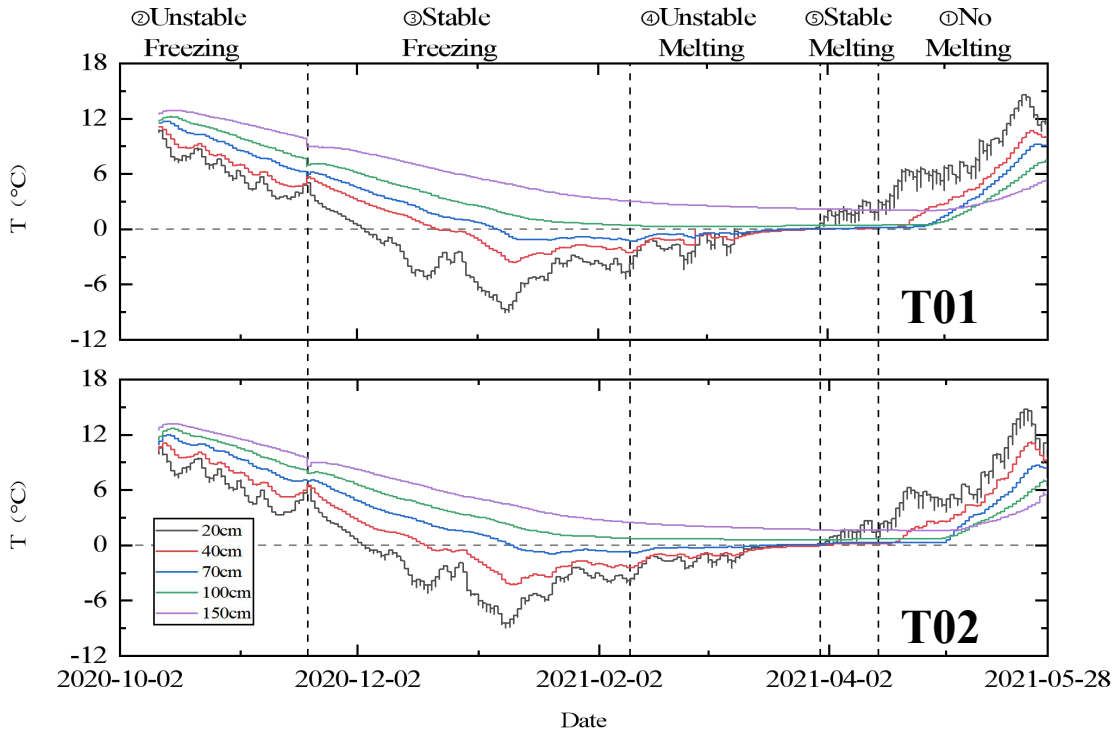

Figure 4. The soil temperature monitoring curves of T01 and T02 at different depths

During the unstable freezing period (from October 1 to November 20, lasting 51 days), the temperature at night gradually goes down below 0°C. The temperature in the different layers fell below 0°C layer by layer. At this stage, soil moisture content decreased sharply after a brief increase which is due to the brief increase in temperature and precipitation.

During the stable freezing period (from November 21 to February 14, lasting 86 days), both the atmospheric day and night temperatures were consistently below 0°C, and the upper soil was gradually frozen steadily after November 21. Affected by the freezing process, the volumetric moisture content of soil showed remarkable declining trends, especially in 20cm and 40cm soil layers. The gravitational water of the soil is completely frozen and the moisture content of the soil reached the lowest value at this stage. At the beginning of the following January, the atmospheric and soil temperatures had minimum valves. However, for some time after January, the soil temperature at the monitoring depths remained below 0 °C (at depths shallower than 70 cm as shown in Figure 3 and Figure 4), and the soil temperature didn't vary significantly with atmospheric temperature, the soil still remained in a stable freezing state.

During the unstable melting period (from February 15 to March 31, lasting 45 days), the atmospheric temperature was above 0°C by February 15 during the day and below 0°C at night. During this period, unliked the stable freezing period, the soil temperature was considerably affected by atmospheric temperature. Soil temperature at 20 cm depth increased evidently. With the increasing air temperature, the freeze-thaw process acted alternately on the soil. Affected by the freeze-thaw process, the moisture content of the upper soil layers (20 and 40 cm) showed a fluctuating upward trend.

During stable melting period (from April 1 to 30, lasting 30 days), the air temperatures continuously increased following April 1. There was only thawing process in the soil and the upper soil was responsive to change in atmospheric temperature most quickly and the temperature of the upper soil layer is gradually higher than that of the lower soil layer.

These data indicated that the freeze-thaw cycle began at October 1, and ended at the end of April. In January, the freezing process reached its maximum. In the freezing period, the upper soil layer temperature was lower than the soil layer below and this situation fot inversely in the thawing period. The soil moisture content in the upper layer was only higher than the soil layer below in the stable melting period. The above phenomenon shows the characteristics of "undirectional freezing, bidirectional melting" which is due to the combined impact of atmospheric temperature change and groundwater energy transmission.

3 Mathematical model

3.1 Governing equations

Table 1. Variable names and their physical meanings

V	volume[L^3]	k	rock intrinsic permeability[m^2]
V_n	volume of subdomain n[L^3]	$k_{r\beta}$	Relative permeability [dimensionless]

M	mass accumulation term of component κ [kg.m^{-3}]	μ_β	viscosity of the aqueous phase[Pa.s]
Γ	surface area[L^2]	P_β	pressure of the aqueous phase[Pa]
Γ_n	surface area of subdomain n [L^2]	$\mathbf{g}$	gravitational acceleration vector[m.s^{-2}]
$\mathbf{F}^\kappa$	Darcy flux vector of component κ [kg.m^{-2}.s^{-1}]	λ	Composite thermal conductivity of the rock-fluids ensemble[W.m^{-1}.K^{-1}]
$\mathbf{n}$	inward unit normal vector	h_β	specific enthalpy of phase β[Jkg^{-1}]
q^κ	source/sink term of component κ [kg.m^{-3}.s^{-1}]	$S_{r\beta}$	correctional relative saturation[dimensionless]
t	time[T]	k_0	original permeability[m^2]
ϕ	porosity[dimensionless]	Γ_f	the fractional length of the pore bodies[dimensionless]
ρ_β	density of phase β[kg.m^{-3}]	ϕ_r	original porosity[dimensionless]
S_β	saturation of phase β[dimensionless]	λ_l	liquid phase thermal conductivity[W.m^{-1}.K^{-1}]
X_β^κ	mass fraction of component κ in phase β[kg/kg]	λ_g	gas phase thermal conductivity[W.m^{-1}.K^{-1}]
N_β	number of phases β[kg/kg]	λ_i	ice phase thermal conductivity[W.m^{-1}.K^{-1}]
N_κ	number of components κ in phase β[kg/kg]	θ_l	liquid phase saturation[dimensionless]
ρ_R	rock density[kg.m^{-3}]	θ_g	gas phase saturation[dimensionless]
C_R	heat capacity of the dry rock[J.kg^{-1}.K^{-1}]	θ_i	ice phase saturation[dimensionless]
u_β	internal energy of phase β[J.kg^{-1}]		

Unlike the traditional groundwater systems, the frozen soil is typically a

multiphase multi-component system, which consists of two components (water and air), existing in three phases (gas, liquid, and ice). From the perspective of the subsurface flow system, the freeze-thaw process is essentially a coupling of multiphase flow and heat transfer. The mutual solubility of components in each phase and the transition between water and ice are all considered. Each phase's properties (such as viscosity, density, and specific enthalpy) are functions of pressure, temperature, and phase composition. The conservation equation could be expressed as Eq(1):

$$\frac{d}{dt}\int_{V_n} M^{\kappa} dV = \int_{\Gamma_n} \mathbf{F}^{\kappa} \bullet \mathbf{n} d\Gamma + \int_{V_n} q^{\kappa} dV \tag{1}$$

On the left side of the equation:

$$M^{\kappa} = \sum_{\beta=1,\ldots,\ N_\beta} \phi S_\beta \rho_\beta X_\beta^{\kappa}, \quad \kappa = 1,\ldots,\ N_\kappa \tag{2}$$

On the right side of the equation:

$$\mathbf{F}_\beta^{\kappa} = -k\frac{k_{r\beta}\rho_A}{\mu_\beta} X_\beta^{\kappa}\left(\nabla P_\beta - \rho_\beta \mathbf{g}\right) + \mathbf{J}_\beta^{\kappa}, \quad \kappa = 1,\ldots,\ N_\kappa \tag{3}$$

The governing equation of energy conservation is:

$$\frac{d}{dt}\int_{V_n} M^{\kappa+1} dV = \int_{\Gamma_n} \mathbf{F}^{\kappa+1} \cdot \mathbf{n} d\Gamma + \int_{V_n} q^{\kappa+1} dV \tag{4}$$

On the left side of the equation:

$$M^{\kappa+1} = (1-\phi)\rho_R C_R T + \sum_{\beta=1,\ldots,\ N_\beta} \phi S_\beta \rho_\beta u_\beta \tag{5}$$

On the right side of the equation:

$$\mathbf{F}^{\kappa+1} = -\lambda \nabla T + \sum_\beta h_\beta F_\beta \tag{6}$$

3.2 Intrinsic permeability equation

The series tube model (Verma and Pruess, 1987) is selected for considering the influence of porosity change on permeability, the model of intrinsic permeability was treated using the series tube model (Verma & Pruess, 1987), and the intrinsic permeability was non-linear with changes in solid phase saturation. The convergent - divergent nature of natural pores can be captured by this model. Channels consist of capillary segments with alternating diameters, as shown in Figure.5.

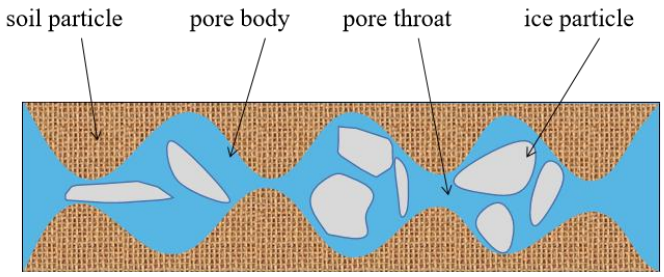

（a）Conceptual model

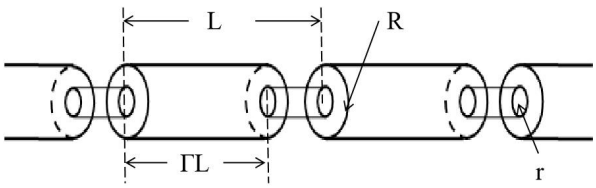

（b）The continuous tube model schematic diagram

Figure 5. The series tube model

In the straight tube model, the permeability remains limited as long as the porosity is not zero, while in the series tube model with different radii, the permeability can decrease to zero when the porosity is not zero due to the thin throat part is occupied by ice. The equation obtained by the model is shown in equation (8).

$$\frac{k}{k_0} = \theta^2 \frac{1-\Gamma_f+\Gamma_f/\omega^2}{1-\Gamma_f+\Gamma_f[\theta/(\theta+\omega-1)]^2} \tag{7}$$

Among them

$$\theta = \frac{1-S_s-\phi_r}{1-\phi_r} \tag{8}$$

$$\omega = 1+\frac{1/\Gamma_f}{1/\phi_r-1} \tag{9}$$

3.3 Relative permeability equation

The addition of relative permeability and capillary pressure could make classic Dary's law apply to the air-water two-phase flow in the unsaturated zone. While, for the frozen-thaw soil, the appearance of ice makes it more complicated by affecting the intrinsic and relative permeability simultaneously. The presence of the ice phase occupies the pore volume, decreasing the available space for fluid flow. Moreover, it changes the liquid phase saturation.

In this study, the relative permeability and capillary pressure model are both selected as van Genuchten's, which are both substantial gas-liquid two-phase models. Hence, for amending the two-phase models to three-phase models and simplification, the ice phase occurrence only affects the intrinsic permeability and the phase saturation of the relative permeability and capillary pressure are independent of other parameters in the models.

Relative permeability is a function of the phase saturation S_β, and $k_{r\beta} = f(S_\beta)$, S_β is the saturation of the phase β and the fraction of the pore space occupied by the phase β. Under the three-phase condition, the formation of ice phase leads to the decrease of the effective pore space for fluid flow, which changes the fraction of the actual pore space occupied by the phase β. If the S_β is still calculated according to

the phase saturation, it will lead to deviation from the actual value. In order to correct this deviation, the relative permeability of gas phase and liquid phase under the three-phase condition is corrected as follows (β is gas phase or liquid phase, $S_{r\beta}$ is the corrected gas phase or liquid phase saturation), then the corrected relative permeability $S_{r\beta}$ of the model is a function of $k_{r\beta} = f(S_{r\beta})$.

$$S_{r\beta} = \frac{S_\beta}{1 - S_i} \tag{10}$$

3.4 Thermal conductivity correction

Effective thermal conductivity describes the ability of soil to transfer heat per unit temperature gradient and is strongly affected by water and ice content, density, texture and temperature. Measuring effective thermal conductivity in frozen soil is difficult and prone to be measured improperly, especially near the freezing or the melting point of soil water (e.g., 4-0°C). Existing steady-state or transient methods for measuring effective thermal conductivity based on the response of soil temperature to external heating tend to lead to soil ice melting and then lead to bias in effective thermal conductivity measurements. Many efforts have been made to develop mathematical algorithms for simulating the thermal conductivity of frozen soils, some of which have been incorporated into numerical simulation programs. He, Flerchinger, Kojima, Dyck, et al. (2021) gave a review in which 39 thermal conductivity models of frozen soil were evaluated and compared， and He, Flerchinger, Kojima, He, et al. (2021) gave an evaluation of 14 thermal conductivity models with observations and SHAW model simulations. Generally, the thermal conductivity of the solid phase is higher than that of the liquid phase, which is higher than gas. The thermal conductivity ranges between 2.1~2.4 W/m/°C for ice, 0.54~0.6 W/m/°C for water, and 0.023 W/m/°C for air. There is an order of magnitude difference between the fluid and ice phases. Therefore, it is necessary to put forward a model that can consider the effect of the proportion change of the liquid-ice-air and the soil skeleton on the effective thermal conductivity. Hence, the following geometric weighted average model considering the proportion change of the liquid-ice-air is implemented in this research.

$$\lambda_e = \lambda_l^{\theta_l} \lambda_g^{\theta_g} \lambda_i^{\theta_i} \tag{11}$$

$$\lambda = \lambda_e \phi + \lambda_s (1 - \phi) \tag{12}$$

3.5 Code development

In IAPWS-IF97, a series of complicated regression equations are derived for calculating the properties of water, steam, and ice based on the primary variables (pressure and temperature) (Figure 7). TOUGH2 keeps the same primary variables as the IAPWS-IF97.

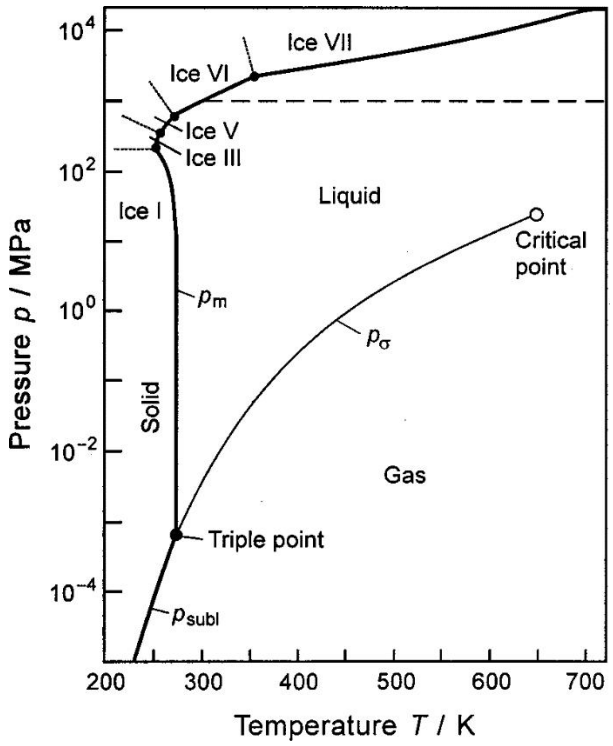

Figure 6. The phase–boundary curves of water in a p – T diagram(Wagner & Pruß, 2002)

This code improvement work is based on the equation of state (EOS) module of EOS3 within the framework of TOUGH2, which is mainly used to describe the gas/water two-phase flow in the unsaturated zone. This study needs to realize the function of the water-ice phase transition.

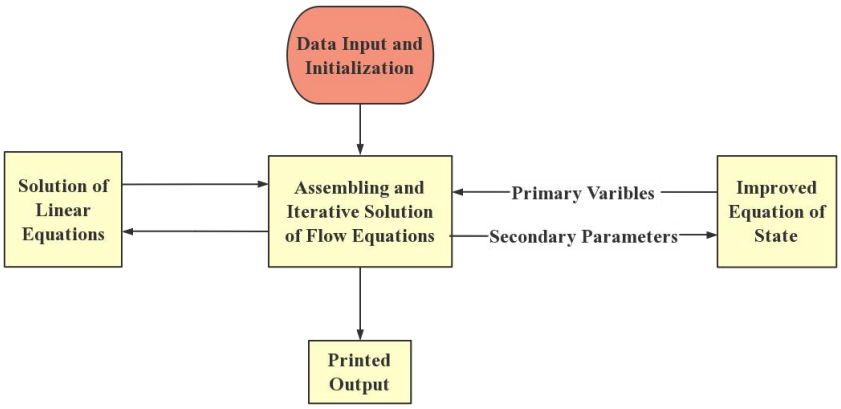

Figure 7. The structure of the development code

First, it needs to determine the number of primary variables to quantify the system. According to the Gibbs phase rule, the freedom degree meets the equation(13). When there exist NPH(number of phases) phases in a system, among which, the saturations of NPH-1 phases are variable to some extent. Hence, it can be deduced that the number of primary variables (NPV) is only decided by the number of components, independent of phase conditions, as Eq(14).

$$F=NK-NPH+2 \tag{13}$$

$$NPV=F+NPH-1=NK+1 \quad (14)$$

Thus, the number of primary variables for this system should be three. Even though the number of primary variables is not limited by the phase conditions, the combinations of the primary variables should be adjusted according to the phase conditions. As shown in Table 2, under single-phase conditions, the primary variable combinations are the pressure, temperature, and mass fraction of air. For two-phase conditions with the air phase, the mass fraction is replaced by the air phase saturation, plus 10, as set in the original TOUGH2-EOS3. Under the conditions of water-ice two-phase, the pressure could be omitted and calculated by the saturation line according to temperature.

Table 2. Primary variables combinations under different phase conditions

Phase	Index	Primary Variables	Possible phase transition
Liquid	1	P, X_g, T	3, 5
Gas	2	P, X_g, T	3, 6
Liquid-Gas	3	P, S_g +10, T	1, 2, 7
Ice	4	P, X_g, T	5, 6
Liquid-Ice	5	Si, X_g, T	1, 4, 7
Gas-Ice	6	P, S_g +10, T	2, 4, 7
Liquid-Gas-Ice	7	S_i, S_g +10, T	3, 5, 6

4. Results and Discussion

4.1 Numerical Model construction

In order to verify the developed model in describing the general pattern of fluid and heat flow in the seasonally frozen soil, a 1-D column model is established based on the measurement on the monitoring site. It is 13m in vertical, starts from the ground surface, and extends downward to the water table. Through particle analysis of the soil sample, the T01 soil type is defined as Baijiang soil (clayey silt), and the T02 soil type is defined as brunisolic soil (sandy soil).

The soil properties, such as porosity, permeability, density, specific heat capacity, and thermal conductivity are all obtained from the measurement of on-site soil samples in the laboratory. The computational domain of the 1-D column is discretized into 60 grids in a 0-3m and 20 grids below 3m, a total of 80 grids. The parameter settings are listed in Table 3.

Table 3. Initial parameter Settings

Parameters	Baijiang soil	brunisolic soil
Matrix density (kg/m^3)	1020	1100
Specific heat capacity (kJ/(kg·K))	1120	1120

Rock Matrix heat conductivity (W/(m·K))	1.8	1.8
Porosity	0.3	0.3
Initial permeability (m^2)	1.0E-9	1.0E-9

The upper boundary is set as the ground surface, and the temperature and rainfall of the boundary are given according to the measured data from the meteorological station. The lower boundary is set as the saturated groundwater with a constant temperature of 25°C. The simulation period was set from October 2, 2020 to May 28, 2021, which covers a whole freeze-thaw period. The initial temperature and moisture distribution along the soil column are also given according to the soil monitored data.

4.2 Temperature and moisture content validation

The measured data at the monitoring sites T01 and T02 between October 2, 2020 and May 28, 2021 were used to verify the soil temperature and water content in different layers, and the results obtained were shown in Figure.9 and Figure.10.

Table 4. The MAE and RMSE values of soil temperature and moisture at different depths

Statistical index	Layer	T01		T02	
		T(℃)	SM(%)	T(℃)	SM(%)
MAE	20cm	1.76	7.15	2.94	5.68
	40cm	0.92	5.10	3.07	4.90
	70cm	0.74	11.87	2.37	6.86
	100cm	1.07	1.85	1.85	1.33
	150cm	0.72	4.13	1.83	1.03
RSME	20cm	2.41	11.61	3.49	7.75
	40cm	1.13	7.81	3.66	8.07
	70cm	1.00	12.69	3.26	8.02
	100cm	1.53	2.25	2.92	1.68
	150cm	1.09	4.76	2.70	1.25

Two statistical indices, MAE and RMSE are employed to compare the measured data with simulated results, which can be seen in Table 4. Obviously the MAE and RSME values of T01 and T02 temperature are lower than 4℃ while the variation scope is 0.72-3.66℃. We have a satisfactory agreement as this difference is much smaller than the amplitude of the annual variations in soil temperature. And we also have a satisfactory agreement as this difference of the MAE and RSME values of T01 and T02 moisture content which the change scope is 1.85%-11.61% and the RSME of 20cm depth in T01 have the max value.

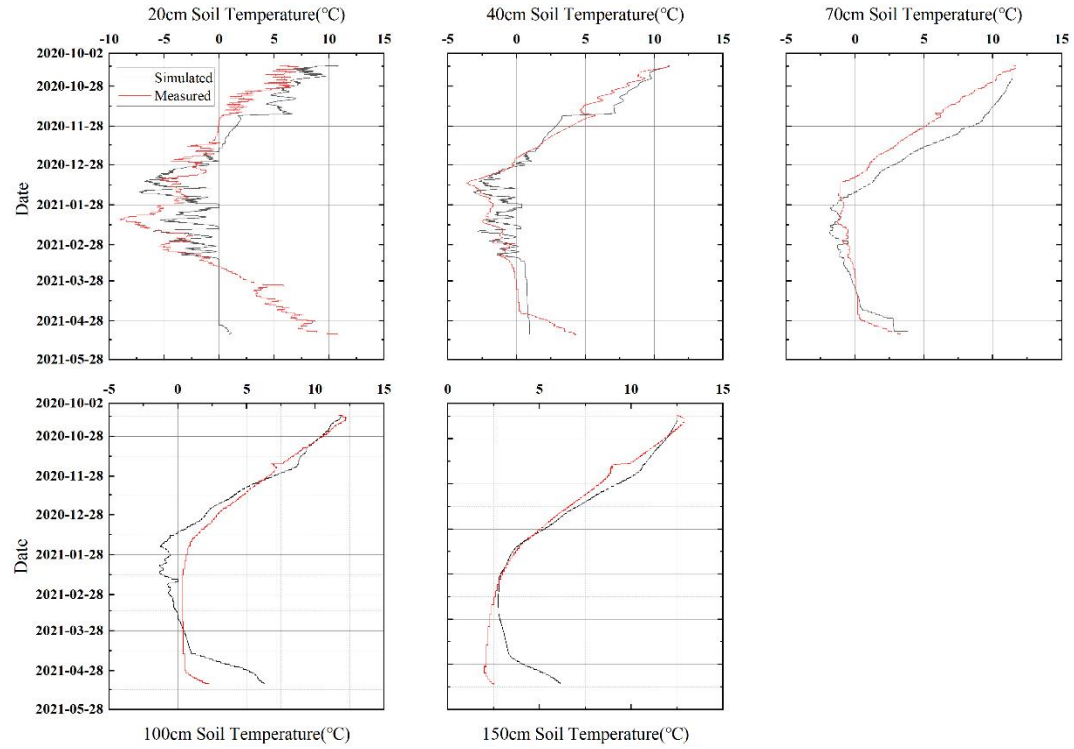

(a) Temperature

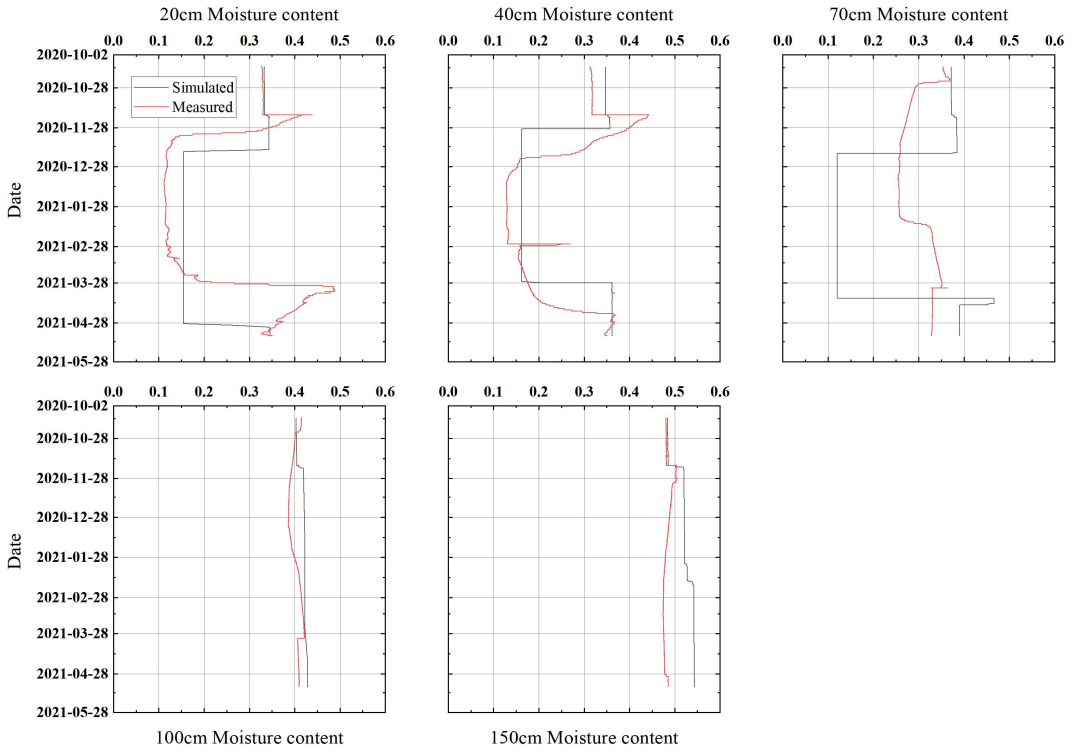

(b) Moisture content

FIG 8. Comparison of simulated and measured data of temperature and moisture content at different soil depths at T01 site

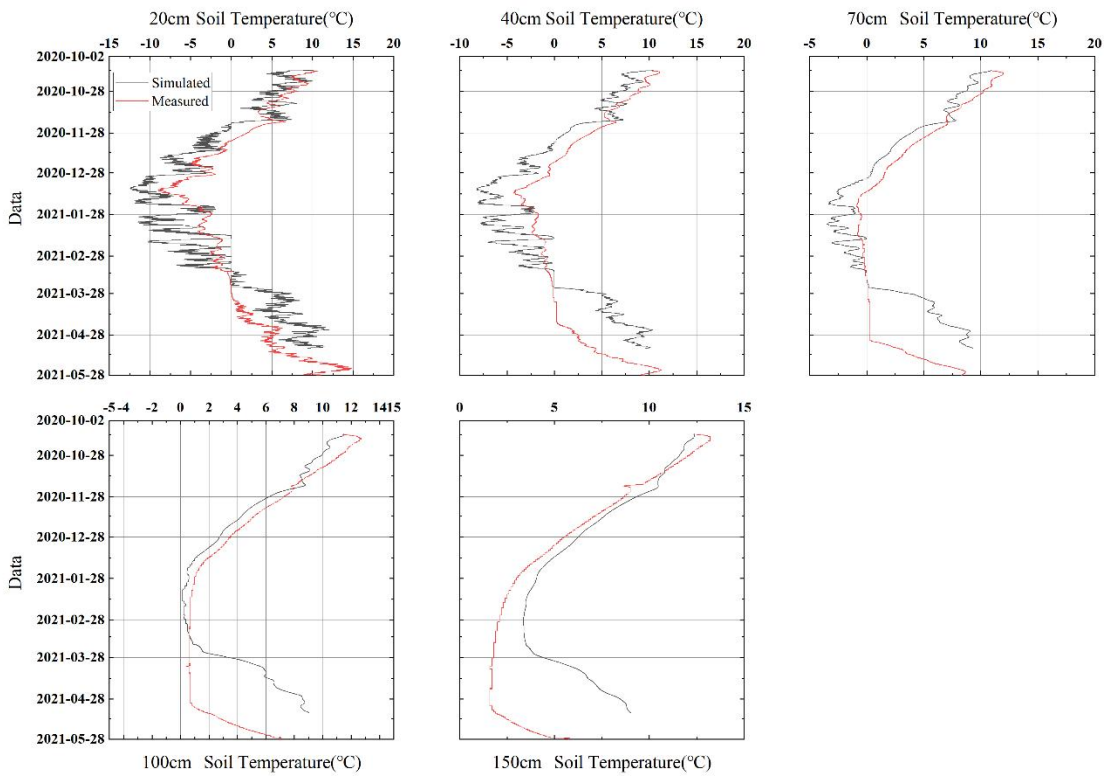

(a) Temperature

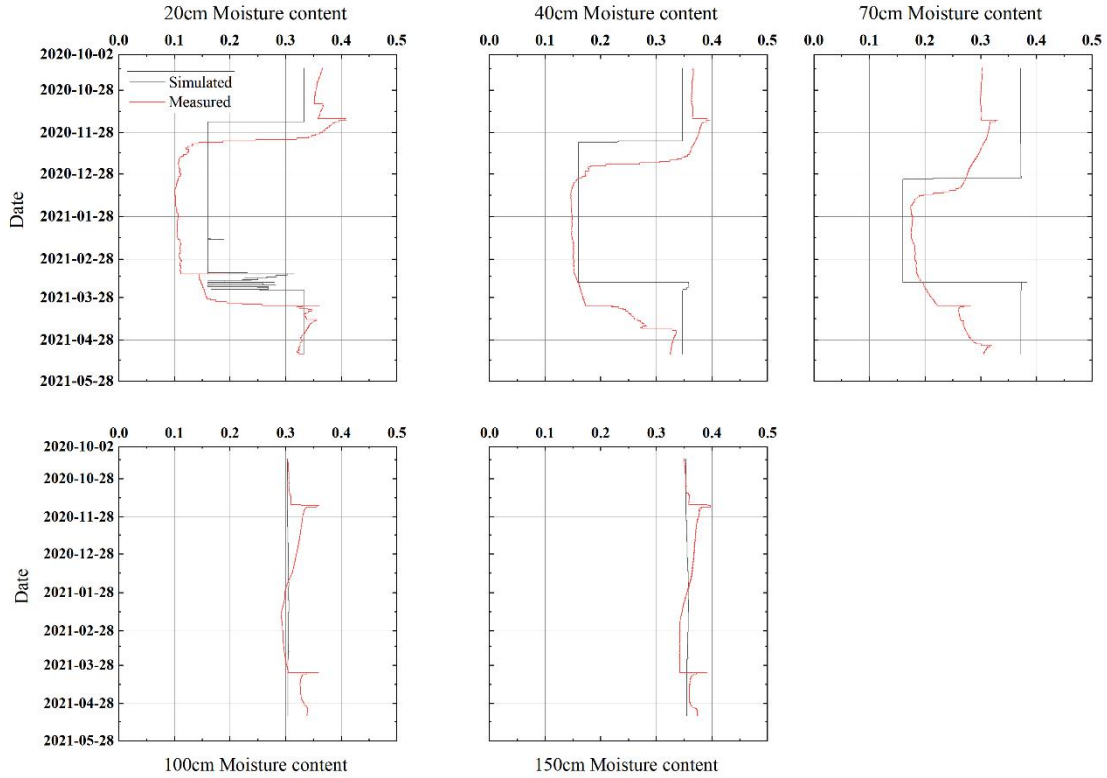

(b) Moisture content

FIG 9. Comparison of simulated and measured data of temperature and moisture content at different soil depths at T02 site

Although the model has a good fitting result for the temperature at the deeper soil layer (100cm and 150cm) during the freezing period, which is slightly higher than the

measured temperature during the melting period. The discrepancies and the lack of volatility may be due to not precise enough estimate of the thermo-hydraulic properties of the soils. Although we already give a strongly physical meaning function of estimation in thermo-hydraulic properties, more accurate results still require direct field measurement and calibration. Another possible reason is the differences between the real soil structure and the simplified geometry domains, which can contain the factors that ignoring frost cracks and heterogeneities of the soil. Moreover, the MAE and RSME in the shallower soil layers is higher than that in the deeper layers, which may be caused by ignoring the effects of snow cover, surface evaporation and sublimation and the sun's radiation.

4.3 Frozen Depth and permeability change

As shown in Figure.11, the envelope curve represents the phase transition temperature (around 0℃) of the seasonal freeze-thaw process, which can be divided into three stages according to the envelope curve. In the first stage, the layers gradually begin to freeze around November 18, 2020, the temperature starts to drop below zero, and the water in the soil starts to freeze. As the temperature dropped dramatically, the frozen depth increased gradually over time, and almost reached a level of linear growth finally. In the second stage, the upper and lower boundary heat flow was basically in a dynamic equilibrium state, the freezing process tended to stabilize and the period of this process is from January 13, 2021 to Mach 10, 2021. At this point, only water-ice phase transition was existing in the layer. The maximum freezing depth is about 1.15m occurred near February 13, 2021 in T01 monitoring site, and 0.97m for T02 on February , 2021. The third stage is a bidirectional melting stage, surface temperature will be back to above 0℃ again, and the negative temperature heat flows to the surface and underground two directions simultaneously, with the heat flow of the underground melt soil boundary, the soil layer begin to melt bidirectional with a rapid progress, a steep curve and a large gradient, which results in a short melting experience time at a start time of March 11, 2021. Around March 11, 2021, the soil began to thaw, and around April 14, 2021, the ice in the soil layer completely melted. The whole freeze-thaw cycle lasted for about 145 days.

In the initial stage of the freezing process in this module, the freezing rate is increasing slowly in the beginning of the freezing process and the freezing depth is gradually close to the linear growth which. For the reason that the water-ice and ice-water phase transition occur alternately, the freezing depth will be limited. Lack of consideration for snow depth and solar radiation could be responsible for such phenomenones When the surface temperature returns to zero, the downward conduction of surface heat flow is overestimated due to the lack of endothermic effects of snowmelt and the blockage of the surface soil and atmosphere by the snow layer.Therefore, we believe that the performance of the coupled model could be further improved by better consideration of the layer of snow. Moreover, plant interception and solar radiation can be added for further improvements of the model.

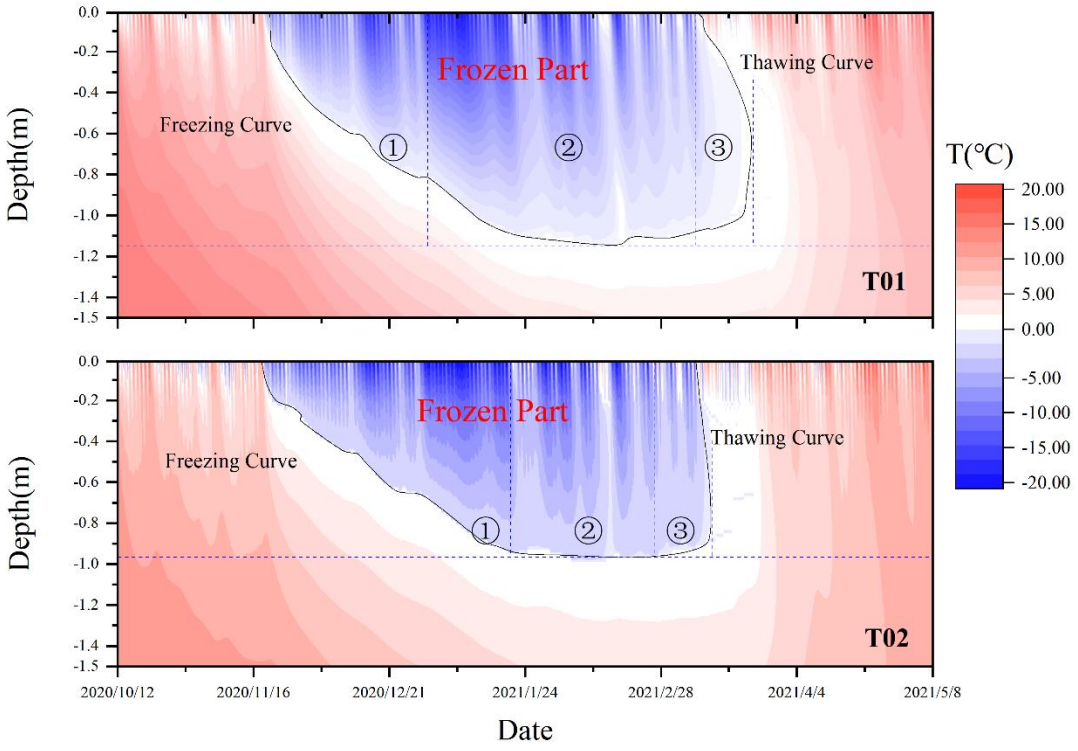

Figure 10. Freeze-thaw process curve in T01 and T02

During the freezing process, the ice phase formed in soil pores, and reduced soil permeability and porosity. Figure.12 shows the evolution process of soil permeability in different soil layers during freeze-thaw period in two monitoring points. In T01 points, the maximum freezing depth obtained by the simulation is 1.15m so that the soil layer above 1.15m will be affected by the recomposition of water-air-ice-soil particle as well as the soil layer above 0.97m in T02. For demonstration purposes, the evolution of permeability in the 150cm layer which will not be affected by the ice phase and isn't shown in Figure.12. As the depth of freezing increases,the soil layer gradually frozen and the permeability decreased layer by layer with the ice phase beginning formation. The variation trend of soil permeability can directly reflects the frozen depth during freezing period of the soil layer, the layers of 20cm, 40cm, 70cm and 100cm layers in T01 were frozen successively but 20cm and 100cm layer thawed firstly with 40cm and 70cm thawing soon afterwards and there is a similar pattern in T02 which shows the characteristics of soil bidirectional melting. According to the equation(8), the influence of ice phase saturation has a significant impact on soil permeability. There is a difference between the minimum value in different depths while the permeability of 70cm layer decreased the most from 2.0E-8 to 6.0E-9 in T01 and to 8.0E-9 in T02 in the freezing stage. The permeability of the soil layer decreased from 1/2 to 1/4 of the original permeability.

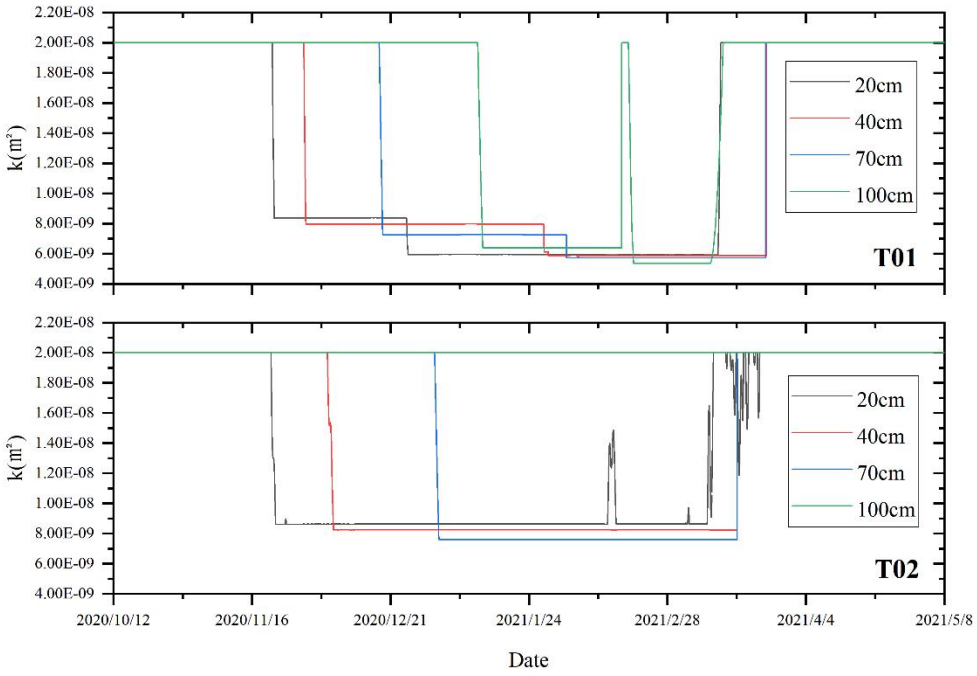

Figure 11. The evolution process of soil permeability in T01 and T02

Hence, the presence of ice would be an impedance in the hydrogeology process in cold regions, especially there will be a greatest ice phase saturation in the frozen intermediate strata. The infiltration in seasonal frozen region would be greatly restricted during the freeze-thaw period.

5. Conclusions

In this reaserach, the insufficient factors of the widely used models are analyzed systematically. A mathematical coupling method completely based on the thermal properties of water is proposed to simulate the freeze-thaw process considering the water-ice phase transition process. A calculation program is developed based on TOUGH2 EOS3 module. The prediction of soil moisture content, temperature distribution and permeability at different depths during water was realized. Tools are provided for the construction of hydrogeological model and the simulation of infiltration process in cold region.

However, the coupling between water phase saturation and temperature change in shallow soil under negative temperature needs to be further improved. On this basis, it is important to further clarify the transport mechanism of shallow soil water and predict the change of unfrozen water content under freeze-thaw conditions.

Acknowledgements

This study was supported by China National Science Foundation (grant No. 42072280), the National Program on Key Research and Development Project (No. 2019YFC0409103). Meteorologicaldata were supported by the Northeast Institute of Geography and Agroecology, Chinese Academy of Sciences.

Reference

Bense, V. F., Ferguson, G., & Kooi, H. (2009). Evolution of shallow groundwater flow systems in areas of degrading permafrost. *Geophysical Research Letters, 36*. https://doi.org/10.1029/2009gl039225

Chen, Y. Q., Zhou, Z. F., Wang, J. G., Zhao, Y., & Dou, Z. (2021). Quantification and division of unfrozen water content during the freezing process and the influence of soil properties by low-field nuclear magnetic resonance. *Journal of Hydrology, 602*. https://doi.org/10.1016/j.jhydrol.2021.126719

Christ, M., & Kim, Y. C. (2009). Experimental study on the physical-mechanical properties of frozen silt. *Ksce Journal of Civil Engineering, 13*(5), 317-324. https://doi.org/10.1007/s12205-009-0317-z

Dagenais, S., Molson, J., Lemieux, J. M., Fortier, R., & Therrien, R. (2020). Coupled cryo-hydrogeological modelling of permafrost dynamics near Umiujaq (Nunavik, Canada). *Hydrogeology Journal, 28*(3), 887-904. https://doi.org/10.1007/s10040-020-02111-3

Dall'Amico, M., Endrizzi, S., Gruber, S., & Rigon, R. (2011). A robust and energy-conserving model of freezing variably-saturated soil. *Cryosphere, 5*(2), 469-484. https://doi.org/10.5194/tc-5-469-2011

Devoie, E. G., Connon, R. F., Craig, J. R., & Quinton, W. L. (2020). Subsurface flow measurements using passive flux meters in variably-saturated cold-regions landscapes. *Hydrological Processes, 34*(23), 4541-4546. https://doi.org/10.1002/hyp.13900

Ebel, B. A., Koch, J. C., & Walvoord, M. A. (2019). Soil Physical, Hydraulic, and Thermal Properties in Interior Alaska, USA: Implications for Hydrologic Response to Thawing Permafrost Conditions. *Water Resources Research, 55*(5), 4427-4447. https://doi.org/10.1029/2018wr023673

Endrizzi, S., Gruber, S., Dall'Amico, M., & Rigon, R. (2014). GEOtop 2.0: simulating the combined energy and water balance at and below the land surface accounting for soil freezing, snow cover and terrain effects. *Geoscientific Model Development, 7*(6), 2831-2857. https://doi.org/10.5194/gmd-7-2831-2014

Evans, S. G., Ge, S. M., Voss, C. I., & Molotch, N. P. (2018). The Role of Frozen Soil in Groundwater Discharge Predictions for Warming Alpine Watersheds. *Water Resources Research, 54*(3), 1599-1615. https://doi.org/10.1002/2017wr022098

Flerchinger, G., & Hanson, C. (1989). MODELING SOIL FREEZING AND THAWING ON A RANGELAND WATERSHED. *Transactions of the ASAE, Vol.32*(No.5), 1551-1554. https://doi.org/10.13031/2013.31188

Frederick, J. M., & Buffett, B. A. (2014). Taliks in relict submarine permafrost andmethane hydrate deposits: Pathways for gas escape under present and future conditions. *Journal of Geophysical Research-Earth Surface, 119*(2), 106-122. https://doi.org/10.1002/2013jf002987

Frederick, J. M., & Buffett, B. A. (2016). Submarine groundwater discharge as a possible formation mechanism for permafrost-associated gas hydrate on the circum-Arctic continental shelf. *Journal of Geophysical Research-Solid Earth,*

121(3), 1383-1404. https://doi.org/10.1002/2015jb012627

Ghias, M. S., Therrien, R., Molson, J., & Lemieux, J. M. (2019). Numerical simulations of shallow groundwater flow and heat transport in continuous permafrost setting under impact of climate warming. *Canadian Geotechnical Journal, 56*(3), 436-448. https://doi.org/10.1139/cgj-2017-0182

Grenier, C., Anbergen, H., Bense, V., Chanzy, Q., Coon, E., Collier, N., et al. (2018). Groundwater flow and heat transport for systems undergoing freeze-thaw: Intercomparison of numerical simulators for 2D test cases. *Advances in Water Resources, 114*, 196-218. https://doi.org/10.1016/j.advwatres.2018.02.001

Grenier, C., Regnier, D., Mouche, E., Benabderrahmane, H., Costard, F., & Davy, P. (2013). Impact of permafrost development on groundwater flow patterns: a numerical study considering freezing cycles on a two-dimensional vertical cut through a generic river-plain system. *Hydrogeology Journal, 21*(1), 257-270. https://doi.org/10.1007/s10040-012-0909-4

Hansson, K., Simunek, J., Mizoguchi, M., Lundin, L. C., & van Genuchten, M. T. (2004). Water flow and heat transport in frozen soil: Numerical solution and freeze-thaw applications. *Vadose Zone Journal, 3*(2), 693-704. https://doi.org/10.2113/3.2.693

Harlan, R. L. (1973). Analysis of coupled heat‐fluid transport in partially frozen soil. *Water Resources Research, Vol.9*(No.5), 1314-1323. https://doi.org/10.1029/WR009i005p01314

He, H. L., Flerchinger, E. A., Kojima, Y., Dyck, M. L., & Lv, J. L. (2021). A review and evaluation of 39 thermal conductivity models for frozen soils. *Geoderma, 382*. https://doi.org/10.1016/j.geoderma.2020.114694

He, H. L., Flerchinger, G. N., Kojima, Y., He, D., Hardegree, S. P., Dyck, M. F., et al. (2021). Evaluation of 14 frozen soil thermal conductivity models with observations and SHAW model simulations. *Geoderma, 403*. https://doi.org/10.1016/j.geoderma.2021.115207

Holmen, J., Benabderrahmane, H., Buoro, A., & Brulhet, J. (2011). Modelling of permafrost freezing and melting and the impact of a climatic cycle on groundwater flow at the Meuse/Haute-Marne site. *Physics and Chemistry of the Earth, 36*(17-18), 1531-1538. https://doi.org/10.1016/j.pce.2011.10.021

Hou, R., Li, T., Fu, Q., Liu, D., Li, M., Zhou, Z., et al. (2020). Effects of biochar and straw on greenhouse gas emission and its response mechanism in seasonally frozen farmland ecosystems. *Catena, 194*, 104735. https://doi.org/10.1016/j.catena.2020.104735

Ireson, A. M., van der Kamp, G., Ferguson, G., Nachshon, U., & Wheater, H. S. (2013). Hydrogeological processes in seasonally frozen northern latitudes: understanding, gaps and challenges. *Hydrogeology Journal, 21*(1), 53-66. https://doi.org/10.1007/s10040-012-0916-5

Karra, S., Painter, S. L., & Lichtner, P. C. (2014). Three-phase numerical model for subsurface hydrology in permafrost-affected regions (PFLOTRAN-ICE v1.0). *Cryosphere, 8*(5), 1935-1950. https://doi.org/10.5194/tc-8-1935-2014

Knighton, J., Souter-Kline, V., Volkmann, T., Troch, P. A., Kim, M., Harman, C. J., et

al. (2019). Seasonal and Topographic Variations in Ecohydrological Separation Within a Small, Temperate, Snow-Influenced Catchment. *Water Resources Research, 55*(8), 6417-6435. https://doi.org/10.1029/2019WR025174

Kong, F., Nie, L., Xu, Y., Rui, X., He, Y., Zhang, T., et al. (2022). Effects of freeze-thaw cycles on the erodibility and microstructure of soda-saline loessal soil in Northeastern China. *Catena, 209*, 105812. https://doi.org/10.1016/j.catena.2021.105812

Kurylyk, B. L., & Hayashi, M. (2016). Improved Stefan Equation Correction Factors to Accommodate Sensible Heat Storage during Soil Freezing or Thawing. *Permafrost and Periglacial Processes, 27*(2), 189-203. https://doi.org/10.1002/ppp.1865

Kurylyk, B. L., Hayashi, M., Quinton, W. L., McKenzie, J. M., & Voss, C. I. (2016). Influence of vertical and lateral heat transfer on permafrost thaw, peatland landscape transition, and groundwater flow. *Water Resources Research, 52*(2), 1286-1305. https://doi.org/10.1002/2015wr018057

Kurylyk, B. L., McKenzie, J. M., MacQuarrie, K. T. B., & Voss, C. I. (2014). Analytical solutions for benchmarking cold regions subsurface water flow and energy transport models: One-dimensional soil thaw with conduction and advection. *Advances in Water Resources, 70*, 172-184. https://doi.org/10.1016/j.advwatres.2014.05.005

Kurylyk, B. L., & Watanabe, K. (2013). The mathematical representation of freezing and thawing processes in variably-saturated, non-deformable soils. *Advances in Water Resources, 60*, 160-177. https://doi.org/10.1016/j.advwatres.2013.07.016

Lamontagne-Halle, P., McKenzie, J. M., Kurylyk, B. L., Molson, J., & Lyon, L. N. (2020). Guidelines for cold-regions groundwater numerical modeling. *Wiley Interdisciplinary Reviews-Water, 7*(6). https://doi.org/10.1002/wat2.1467

Langford, J. E., Schincariol, R. A., Nagare, R. M., Quinton, W. L., & Mohammed, A. A. (2020). Transient and Transition Factors in Modeling Permafrost Thaw and Groundwater Flow. *Groundwater, 58*(2), 258-268. https://doi.org/10.1111/gwat.12903

Liu, W., Fortier, R., Molson, J., & Lemieux, J.-M. (2022). Three-Dimensional Numerical Modeling of Cryo-Hydrogeological Processes in a River-Talik System in a Continuous Permafrost Environment. *Water Resources Research, 58*(3), e2021WR031630. https://doi.org/10.1029/2021WR031630

McKenzie, J. M., Voss, C. I., & Siegel, D. I. (2007). Groundwater flow with energy transport and water-ice phase change: Numerical simulations, benchmarks, and application to freezing in peat bogs. *Advances in Water Resources, 30*(4), 966-983. https://doi.org/10.1016/j.advwatres.2006.08.008

Mohammed, A. A., Bense, V. F., Kurylyk, B. L., Jamieson, R. C., Johnston, L. H., & Jackson, A. J. (2021). Modeling Reactive Solute Transport in Permafrost-Affected Groundwater Systems. *Water Resources Research, 57*(7), e2020WR028771. https://doi.org/10.1029/2020WR028771

Nagare, R. M., Schincariol, R. A., Quinton, W. L., & Hayashi, M. (2012). Effects of

freezing on soil temperature, freezing front propagation and moisture redistribution in peat: laboratory investigations. *Hydrology and Earth System Sciences, 16*(2), 501-515. https://doi.org/10.5194/hess-16-501-2012

Nikolaev, P., Sedighi, M., Jivkov, A. P., & Margetts, L. (2022). Analysis of heat transfer and water flow with phase change in saturated porous media by bond-based peridynamics. *International Journal of Heat and Mass Transfer, 185*. https://doi.org/10.1016/j.ijheatmasstransfer.2021.122327

Orakoglu, M. E., Liu, J. K., & Niu, F. J. (2016). Experimental and modeling investigation of the thermal conductivity of fiber-reinforced soil subjected to freeze-thaw cycles. *Applied Thermal Engineering, 108*, 824-832. https://doi.org/10.1016/j.applthermaleng.2016.07.112

Orgogozo, L., Prokushkin, A. S., Pokrovsky, O. S., Grenier, C., Quintard, M., Viers, J., & Audry, S. (2019). Water and energy transfer modeling in a permafrost-dominated, forested catchment of Central Siberia: The key role of rooting depth. *Permafrost and Periglacial Processes, 30*(2), 75-89. https://doi.org/10.1002/ppp.1995

Painter, S. L. (2011). Three-phase numerical model of water migration in partially frozen geological media: model formulation, validation, and applications. *Computational Geosciences, 15*(1), 69-85. https://doi.org/10.1007/s10596-010-9197-z

Painter, S. L., Coon, E. T., Atchley, A. L., Berndt, M., Garimella, R., Moulton, J. D., et al. (2016). Integrated surface/subsurface permafrost thermal hydrology: Model formulation and proof-of-concept simulations. *Water Resources Research, 52*(8), 6062-6077. https://doi.org/10.1002/2015wr018427

Painter, S. L., Moulton, J. D., & Wilson, C. J. (2013). Modeling challenges for predicting hydrologic response to degrading permafrost. *Hydrogeology Journal, 21*(1), 221-224. https://doi.org/10.1007/s10040-012-0917-4

Peng, Z., Tian, F., Wu, J., Huang, J., Hu, H., & Darnault, C. J. G. (2016). A numerical model for water and heat transport in freezing soils with nonequilibrium ice-water interfaces. *Water Resources Research, 52*(9), 7366-7381. https://doi.org/10.1002/2016WR019116

Philip, J. R., & Vries, D. A. D. (1957). Moisture movement in porous materials under temperature gradients. *Transactions, American Geophysical Union, Vol.38*(No.2), 222-232. https://doi.org/10.1029/TR038i002p00222

Riviere, A., Jost, A., Goncalves, J., & Font, M. (2019). Pore water pressure evolution below a freezing front under saturated conditions: Large-scale laboratory experiment and numerical investigation. *Cold Regions Science and Technology, 158*, 76-94. https://doi.org/10.1016/j.coldregions.2018.11.005

Rush, M. J., & Rajaram, H. (2022). Influence of Snowpack Cold Content on Seasonally Frozen Ground and Its Hydrologic Consequences: A Case Study From Niwot Ridge, CO. *Water Resources Research, 58*(9), e2021WR031911. https://doi.org/10.1029/2021WR031911

Scheidegger, J. M., Jackson, C. R., McEvoy, F. M., & Norris, S. (2019). Modelling permafrost thickness in Great Britain over glacial cycles. *Science of the Total*

Environment, 666, 928-943. https://doi.org/10.1016/j.scitotenv.2019.02.152

Seyedrahimi-Niaraq, M., Doulati Ardejani, F., Noorollahi, Y., Jalili Nasrabadi, S., & Hekmatnejad, A. (2021). An unsaturated three-dimensional model of fluid flow and heat transfer in NW Sabalan geothermal reservoir. *Geothermics, 89*, 101966. https://doi.org/10.1016/j.geothermics.2020.101966

Sjoberg, Y., Coon, E., Sannel, A. B. K., Pannetier, R., Harp, D., Frampton, A., et al. (2016). Thermal effects of groundwater flow through subarctic fens: A case study based on field observations and numerical modeling. *Water Resources Research, 52*(3), 1591-1606. https://doi.org/10.1002/2015wr017571

Stuurop, J. C., van der Zee, S., Voss, C. I., & French, H. K. (2021). Simulating water and heat transport with freezing and cryosuction in unsaturated soil: Comparing an empirical, semi-empirical and physically-based approach. *Advances in Water Resources, 149*. https://doi.org/10.1016/j.advwatres.2021.103846

Sun, B., Liu, J., Ren, F., Li, H., Zhang, G., Ma, J., et al. (2022). Effects of seasonal freeze–thaw and wind erosion on runoff and sediment yields of three loamy slopes of Loess Plateau, China. *Catena, 215*, 106309. https://doi.org/10.1016/j.catena.2022.106309

Sun, D.-m., Li, X.-m., Feng, P., & Zang, Y.-g. (2016). Stability analysis of unsaturated soil slope during rainfall infiltration using coupled liquid-gas-solid three-phase model. *Water Science and Engineering, 9*(3), 183-194. https://doi.org/10.1016/j.wse.2016.06.008

Sun, Y., Liu, Z., Li, Q., Deng, S., & Guo, W. (2019). Controlling groundwater infiltration by gas flooding for oil shale in situ pyrolysis exploitation. *Journal of Petroleum Science and Engineering, 179*, 444-454. https://doi.org/10.1016/j.petrol.2019.04.055

Sutton, O. F., & Price, J. S. (2020). Modelling the hydrologic effects of vegetation growth on the long-term trajectory of a reclamation watershed. *Science of the Total Environment, 734*. https://doi.org/10.1016/j.scitotenv.2020.139323

Verma, A., & Pruess, K. (1987). 40 – Effects of Silica Redistribution on Performance of High-Level Nuclear Waste Repositories in Saturated Geologic Formations. *Coupled Processes Associated with Nuclear Waste Repositories*, 541-563. https://doi.org/10.1016/B978-0-12-701620-7.50043-X

Wagner, W., & Pruß, A. (2002). The IAPWS Formulation 1995 for the Thermodynamic Properties of Ordinary Water Substance for General and Scientific Use. *Journal of Physical and Chemical Reference Data, Vol.31*(No.2), 387-535. https://doi.org/10.1063/1.1461829

Walvoord, M. A., & Kurylyk, B. L. (2016). Hydrologic Impacts of Thawing Permafrost-A Review. *Vadose Zone Journal, 15*(6). https://doi.org/10.2136/vzj2016.01.0010

Walvoord, M. A., Voss, C. I., & Wellman, T. P. (2012). Influence of permafrost distribution on groundwater flow in the context of climate-driven permafrost thaw: Example from Yukon Flats Basin, Alaska, United States. *Water Resources Research, 48*. https://doi.org/10.1029/2011wr011595

Wang, D. Y., Wang, Y. T., Ma, W., Lei, L. L., & Wen, Z. (2018). Study on the freezing-induced soil moisture redistribution under the applied high pressure. *Cold Regions Science and Technology, 145*, 135-141. https://doi.org/10.1016/j.coldregions.2017.10.012

Wang, H., Wang, F., Sun, J., Cheng, Z., Wang, Y., & Cao, Y. (2023). New strategy for evaluating the spatiotemporal distribution of groundwater resource quantity under seasonal freeze/thaw in mountainous areas. *Journal of Hydrology, 616*, 128850. https://doi.org/10.1016/j.jhydrol.2022.128850

Wang, L., Liu, J., Yu, X., Wang, T., & Feng, R. (2021). A Simplified Model for the Phase Composition Curve of Saline Soils Considering the Second Phase Transition. *Water Resources Research, 57*(1), e2020WR028556. https://doi.org/10.1029/2020WR028556

Wang, X., Wang, C., Wang, X., & Huo, Z. (2020). Response of soil compaction to the seasonal freezing-thawing process and the key controlling factors. *Catena, 184*, 104247. https://doi.org/10.1016/j.catena.2019.104247

Yi, X. Y., Su, D. Y., Seigneur, N., & Mayer, K. U. (2021). Modeling of Thermal-Hydrological-Chemical (THC) Processes During Waste Rock Weathering Under Permafrost Conditions. *Frontiers in Water, 3*. https://doi.org/10.3389/frwa.2021.645675

Zhang, C. Y., Chen, F., Sun, L., Ma, Z. C., & Yao, Y. (2021). A new seasonal frozen soil water-thermal coupled migration model and its numerical simulation. *Plos One, 16*(11). https://doi.org/10.1371/journal.pone.0258861

Zhao, Y., Si, B. C., He, H. L., Xu, J. H., Peth, S., & Horn, R. (2016). Modeling of Coupled Water and Heat Transfer in Freezing and Thawing Soils, Inner Mongolia. *Water, 8*(10). https://doi.org/10.3390/w8100424